
A Nonparametric Bayesian Model for Sparse Temporal Multigraphs

Elahe Ghalebi
TU Wien

Hamidreza Mahyar
Boston University

Radu Grosu
TU Wien

Graham W. Taylor
University of Guelph
Vector Institute for Artificial Intelligence

Sinead A. Williamson
University of Texas, Austin

Abstract

As the availability and importance of temporal interaction data—such as email communication—increases, it becomes increasingly important to understand the underlying structure that underpins these interactions. Often these interactions form a multigraph, where we might have multiple interactions between two entities. Such multigraphs tend to be sparse yet structured, and their distribution often evolves over time. Existing statistical models with interpretable parameters can capture some, but not all, of these properties. We propose a dynamic nonparametric model for interaction multigraphs that combines the sparsity of edge-exchangeable multigraphs with dynamic clustering patterns that tend to reinforce recent behavioral patterns. We show that our method yields improved held-out likelihood over stationary variants, and impressive predictive performance against a range of state-of-the-art dynamic graph models.

1 Introduction

Many forms of social interaction can be represented in terms of a multigraph—*i.e.* a graph where there can be multiple edges between two vertices. For example, vertices might correspond to individuals, with each edge representing an email between two individuals. In large-scale applications, such multigraphs are typically

sparse, with the number of edges being small relative to the number of unconnected pairs of vertices.

Edge-exchangeable models (Cai et al., 2016; Crane & Dempsey, 2018) have been proposed as models for sparse multigraphs, and clustering-based edge-exchangeable models allow the incorporation of community-type structure, (Williamson, 2016). Such models assume that we will see more edges and vertices in future, making them appropriate for growing graphs. However they assume that the distribution is stationary, and that the resulting multigraph is invariant to reordering the arrival times of the edges. In practice, most real-world multigraphs will be dynamic, with the underlying distribution dynamically evolving. For example, topics of communication may wax and wane in popularity, and the set of individuals interested in a given topic may evolve over time.

We propose a new model for dynamic multigraphs, the Dynamic Nonparametric Network Distribution (DYNPAND). The DYNPAND uses a hierarchical clustering mechanism to capture interaction patterns within the multigraph, and uses distance-dependent Chinese Restaurant Processes (ddCRPs Blei & Frazier, 2011) to incorporate temporal dynamics by preferentially assigning edges to clusters and vertices that have been recently active. This dynamic mechanism, in combination with a Pitman-Yor process-distributed base measure ensures our model is appropriate for both sparse and dense multigraphs, with the degree of sparsity controlled by a single parameter. The increased flexibility allowed by our model leads to improved performance over both its exchangeable counterpart and a range of state-of-the-art dynamic network models.

We begin in Section 2 by providing a general introduction to Bayesian models for multigraphs, in both stationary and dynamic setting, plus a review of the distributions (*i.e.* ddCRP and Pitman-Yor process) used in the remainder of the paper. We then intro-

duce our dynamic Bayesian model for sparse temporal multigraphs in Section 3, and discuss the inference in Section 4. In Section 5, we experimentally evaluate the performance of our model both held-out edge prediction and graph forecasting tasks, demonstrating improved performance over state-of-the-art Bayesian methods.

2 Background and Related Work

Our goal is to construct a Bayesian model for sparse multigraphs where interaction patterns can vary over time. Like many dynamic graph models, our model extends an existing stationary model to include temporal dynamics, thus leveraging desirable properties of the underlying stationary model. To provide appropriate context, in this section we discuss existing Bayesian models for multigraphs in the stationary (Section 2.1) and dynamic (Section 2.2) setting. We end this section by reviewing the ddCRP and the Pitman-Yor process, which will be used in our construction.

2.1 Bayesian models for multigraphs

Bayesian models for multigraphs can loosely be divided into three camps. Most common are models where the value of an edge between vertices u and v is a random variable parameterized by the value of some function $\theta(u, v)$. In the multigraph setting, we consider in this paper, that function might be a Poisson distribution. We refer to the resulting multigraphs as jointly vertex-exchangeable (Aldous, 1981; Hoover, 1979; Orbanz & Roy, 2014), since the distribution over the adjacency matrix is invariant to jointly permuting the row and column indices. This class includes the stochastic block-model (Snijders & Nowicki, 1997; Karrer & Newman, 2011); the infinite relational model (Kemp et al., 2006); the mixed-membership stochastic blockmodel (Airoldi et al., 2008); the Latent Feature Relational Model (Miller et al., 2009); and Poisson factor analysis (Zhou & Carin, 2013; Gopalan et al., 2015). While these models are able to capture interesting community structure, the resulting graphs are dense almost surely, (Aldous, 1981; Hoover, 1979). This makes them a poor choice for large real-world multigraphs, which are typically sparse. Further, they assume zero-valued edges are explicitly observed, making them poorly suited for many prediction tasks.

Second, we have multigraphs where the edges are distributed according to a Poisson process on the space of potential edges. A canonical example of such a model is the sparse exchangeable multigraph of Caron & Fox (2017), where the edges are sampled according to a Poisson process whose rate measure is distributed according to a generalized gamma process. Lee et al. (2018) is an extension of such a model with community structure.

These models yield sparse graphs with power-law degree distribution, properties that are common in large social networks. However, like the vertex-exchangeable graphs, they assume a fully observed graph where no new edges will be seen between existing vertices, making them poorly suited to prediction tasks.

Third, we have multigraphs constructed using an exchangeable sequence of edges (Cai et al., 2016; Crane & Dempsey, 2018; Williamson, 2016). Here, we assume the edges are generated by sequentially sampling pairs of vertices. These pairs of vertices are *iid* given some nonparametric prior, such as a Dirichlet process (DP), (Williamson, 2016), a normalized generalized gamma process, (Cai et al., 2016), or a Pitman-Yor process, (Crane & Dempsey, 2018). Under certain conditions on this prior, the resulting multigraphs will be sparse, (Cai et al., 2016; Crane & Dempsey, 2018). Unlike the vertex-exchangeable and Poisson process based models, edge exchangeable multigraphs can grow over time by adding new edges, either between new or previously seen vertices. For this reason, we focus on edge-exchangeable graphs in our model development.

2.1.1 Mixture of Dirichlet Network Distributions

While edge-exchangeable models based on a single distribution have desirable sparsity and degree distribution properties, and are appropriate for growing graphs, they lack community-type structure. The mixture of Dirichlet network distributions (MDND, Williamson, 2016) uses a mixture of edge-exchangeable models, with shared infinite-dimensional support. Each edge i is associated with a cluster z_i , governing which edge-exchangeable model it is generated from. The z_i are distributed according to a Chinese restaurant process (CRP), which describes the distribution over partitions in a DP mixture model, allowing an unbounded number of clusters.

Within the k -th cluster, each edge is associated with two “tables”, $b_i^{(s)}$ and $b_i^{(r)}$, sampled from two separate CRPs.¹ These tables are associated with the sender and recipient of the edge, respectively. Each table $b_i^{(s)}$ (or $b_i^{(r)}$) in cluster k is linked with a vertex $\phi_{k,b_i}^{(s)}$ (or $\phi_{k,b_i}^{(r)}$), so that, for example, all edges i where $z_i = k$ and $b_i^{(s)} = c$ have the same sender $\phi_{k,c}^{(s)}$. To ensure that the cluster-specific multigraphs have common support, the vertices for each table are sampled from a global, DP-distributed probability measure H , that is shared across all clusters. The overall distribution over the

¹While the original MDND paper describes this distribution in terms of Dirichlet processes, we will provide an equivalent construction in terms of CRPs, to provide consistency with later contributions.

i th directed edge (s_i, r_i) can be written as

$$\begin{aligned}
 H &\sim \text{DP}(\gamma, \Theta) \\
 P(z_i = k | z_{<i}) &\propto \begin{cases} m_k & k \leq K_+ \\ \alpha & k = K_+ + 1 \end{cases} \\
 P(b_i^{(s)} = c | z_i = k, b_{<i}^{(s)}) &\propto \begin{cases} \rho_{k,c}^{(s)} & c \leq C_{k+}^{(s)} \\ \tau & k = C_{k+}^{(s)} + 1 \end{cases} \quad (1) \\
 P(b_i^{(r)} = c | z_i = k, b_{<i}^{(r)}) &\propto \begin{cases} \rho_{k,c}^{(r)} & c \leq C_{k+}^{(r)} \\ \tau & k = C_{k+}^{(r)} + 1 \end{cases} \\
 \phi_{k,c}^{(s)} &\sim H & s_i &= \phi_{z_i, b_i}^{(s)} \\
 \phi_{k,c}^{(r)} &\sim H & r_i &= \phi_{z_i, b_i}^{(r)}
 \end{aligned}$$

where m_k is the number of times we have seen cluster k ; $z_{<i} = (z_1, \dots, z_{i-1})$; $s_i(r_i)$ is the sender(recipient) of edge i ; $\rho_{k,c}^{(s)}$ is the number of senders sat at table c in cluster k (with $\rho_{k,c}^{(r)}$ defined analogously); K_+ is the number of previously seen clusters; and $C_{k+}^{(s)}$ and $C_{k+}^{(r)}$ are the number of previously seen sender and recipient tables, respectively, in cluster k . Here, $\alpha > 0$ controls the number of clusters, $\gamma > 0$ controls the overall number of vertices, τ controls similarity between clusters, and Θ is some diffuse measure on the space of vertices.

The resulting model exhibits structure due to the clustering of edges. Both the distribution over clusters, and the distribution over edges within a cluster, are exchangeable. While the use of CRPs (as opposed to heavier-tailed distributions such as Pitman-Yor processes and normalized generalized gamma processes) allows for straightforward inference, they mean that the MDND does not yield sparse graphs.

2.2 Models for dynamic graphs

There has been significant research attention on dynamic network modelling. A common approach relies on the extensions of *stationary* network models to a *dynamic* framework. Here we focus on Bayesian models as these are most relevant to the work in hand, but we note that there have been many dynamic extensions of non-Bayesian models such as the exponential random graph model (Guo et al., 2007) and matrix and tensor factorization-based methods (Dunlavy et al., 2011).

Most dynamic Bayesian networks extend jointly vertex-exchangeable graphs. For example, Xu & Hero (2014) extends the stochastic blockmodel using an extended Kalman filter based algorithm; Durante & Dunson (2014) allows parameters to evolve according to stochastic processes; and Xu (2015) relaxes a hidden Markov assumption on the edge-level dynamics, allowing the presence or absence of edges to directly influence fu-

ture edge probabilities. Several methods have also been used to incorporate temporal dynamics into the mixed membership stochastic blockmodel framework (Fu et al., 2009; Xing et al., 2010; Ho et al., 2011), the infinite relational model (Ng & Silva, 2017) and the latent feature relational model (Foulds et al., 2011; Heaukulani & Ghahramani, 2013; Kim & Leskovec, 2013). Most recently, several models have extended Poisson factor analysis. The dynamic gamma process Poisson factorization (DGPPF, Acharya et al., 2015) introduces dependency by incorporating a Markov chain of marginally gamma random variables into the latent representation. The dynamic Poisson gamma model (DPGM, Yang & Koepl, 2018b) extends a bilinear form of Poisson factor analysis (Zhou, 2015) in a similar manner. The dynamic relational gamma process model (DRGPM, Yang & Koepl, 2018a) also incorporates a temporally dependent thinning process.

Much less work has been carried out on dynamic extensions of the sparse graphs generated using Poisson processes or via a sequence of exchangeable edges. In the Poisson process-based space, Palla et al. (2016) uses a time-dependent base measure, and assume edges have a geometric lifespan. In the edge exchangeable case, Ng & Silva (2017) incorporates temporal dynamics into the MDND by introducing a latent Gaussian Markov chain, and a Poisson vertex birth mechanism. Ghalebi et al. (2018) extends the MDND to partially observed data and uses a temporally informed inference algorithm, but the underlying model is stationary.

2.3 Distance-dependent Chinese restaurant process

Under the MDND both the distribution over clusters, and the distributions over sender and recipient vertices within each cluster, are exchangeable. A natural way to incorporate temporal dependence in such a model is to replace the associated CRPs with temporally varying clustering mechanisms. Several models add temporal dynamics to the DP and/or CRP, *e.g.* MacEachern (2000); Lin et al. (2010); Ren et al. (2008). For our purposes, we choose to use the distance-dependent CRP (ddCRP) (Blei & Frazier, 2011).

Under the ddCRP with concentration parameter α and non-negative, non-increasing decay function f such that $f(\infty) = 0$, the probability of an observation x_i joining a cluster k is,

$$P(z_i = k | z_{<i}) \propto \begin{cases} \sum_{j:z_j=k} f(d_{i,j}) & k \leq K_+ \\ \alpha & k = K_+ + 1 \end{cases}$$

where K_+ is the number of previously seen clusters;

$$d_{i,j} = \begin{cases} t_i - t_j & t_i \geq t_j \\ \infty & \text{otherwise} \end{cases} \quad (2)$$

captures how much time has elapsed between x_i and x_j ; and the concentration parameter α controls the expected number of clusters.

2.4 Pitman-Yor process

The DP distribution over H and the CRPs used to assign edges to tables do not have sufficiently heavy tails to yield sparse multigraphs (see Cai et al. (2016) and Crane & Dempsey (2018)). The Pitman-Yor process (Pitman et al., 1997) is an alternative distribution over probability distributions that has heavier tails than the DP. The Pitman-Yor process has previously been used in the construction of sparse, edge-exchangeable multigraphs, albeit without the structure of the MDND (Crane & Dempsey, 2018).

The exchangeable distribution over partitions implied by the Pitman-Yor process can be described using a two-parameter CRP. With discount parameter $0 \leq \sigma < 1$ and concentration parameter $\gamma > -\sigma$, the clustering behavior of the two-parameter CRP is given by

$$P(z_i = k | z_{<i}) \propto \begin{cases} m_k - \sigma & k \leq K_+ \\ \gamma + \sigma K_+ & k = K_+ + 1 \end{cases} \quad (3)$$

where K_+ is the number of existing clusters and m_k is number of times we have seen cluster k . If $\sigma = 0$, this reduces to the standard CRP with concentration parameter γ ; as σ increases, the distribution has increasingly heavy tails.

3 A new model for multigraphs with temporal dynamics

The MDND, described in Section 2.1, assumes that the observed edges are exchangeable—*i.e.*, that the probability of the graph is invariant to reordering of the edge arrival times. This obviously limits their application to dynamically growing graphs, where the underlying mechanism is non-stationary. Further, since it is based on DPs rather than heavier-tailed distributions such as the normalized generalized gamma process or the Pitman-Yor process, it does not concentrate on sparse graphs for any parameter settings.

Inspired by the MDND, we propose a new model, Dynamic Nonparametric Network Distribution (DYNPAND), for dynamic multigraphs with community structure. DYNPAND replaces the Dirichlet process-distributed random measures in Equation (1) with distributions that are either temporally varying, or have heavy tails. As we show in this section, the resulting time-evolving models can capture both sparse and dense multigraphs, depending on the hyperparameters.

Recall that the MDND uses DPs or CRPs in three parts

of its construction (see Equation (1)): $H \sim \text{DP}(\gamma, \Theta)$ controls the number of vertices, and their overall popularity within the graph. CRPs parametrized by τ determine the tables at which senders and recipients sit, in turn controlling the cluster-specific distributions over the “sender” and “recipient” of edges in the graph. Finally, a CRP parametrized by α governs the clustering structure of the edges.

We replace the top-level DP with a Pitman-Yor process, which increases the probability of adding previously unseen vertices. We replace the CRP controlling the overall clustering with a ddCRP with decay function f_1 , and the CRPs controlling the cluster-specific table allocations with ddCRPs with decay function f_2 .

The resulting temporal dependency means that both the cluster probabilities, and the cluster-specific distributions over vertices, can evolve over time. The resulting generative process over directed edges (s_i, r_i) takes the form

$$\begin{aligned} H &:= \sum_{i=1}^{\infty} h_i \delta_{\theta_i} \sim \text{PY}(\gamma, \sigma, \Theta) \\ P(z_i = z | z_{<i}) &\propto \begin{cases} \sum_{j:z_j=z} f_1(d_{i,j}) & k \leq K_+ + 1 \\ \alpha & k = K_+ \end{cases} \\ s_i | z_i, s_{<i}, H &\begin{cases} = s & \text{w.p.} \propto \sum_{j:z_j=z_i, s_j=s} f_2(d_{i,j}) \\ \sim H & \text{w.p.} \propto \tau \end{cases} \\ r_i | z_i, r_{<i}, H &\begin{cases} = r & \text{w.p.} \propto \sum_{j:z_j=z_i, r_j=r} f_2(d_{i,j}) \\ \sim H & \text{w.p.} \propto \tau \end{cases} \end{aligned} \quad (4)$$

where K_+ is the number of previously seen clusters. The hyperparameters α , γ and τ influence the number of clusters and components in a manner analogous to Equation 1; the parameter $\sigma \in [0, 1)$ controls the sparsity of the multigraph, as we will explore in Section 3.1. To reduce the expected number of loops (edges with repeat vertices), we specify our distance as

$$d_{i,j} = \begin{cases} t_i - t_j & t_i \geq t_j, i \neq j \\ \infty & \text{otherwise,} \end{cases} \quad (5)$$

3.1 Sparsity of the resulting graph

In this section, we show that, under mild conditions, if $\sigma > 0.5$ the model described by Equation (4) yields sparse multigraphs. Following Cai et al. (2016), we define a multigraph as sparse if the number of edges grows sub-quadratically with the number of vertices. Throughout, we make the following assumption on decay functions used in ddCRP.

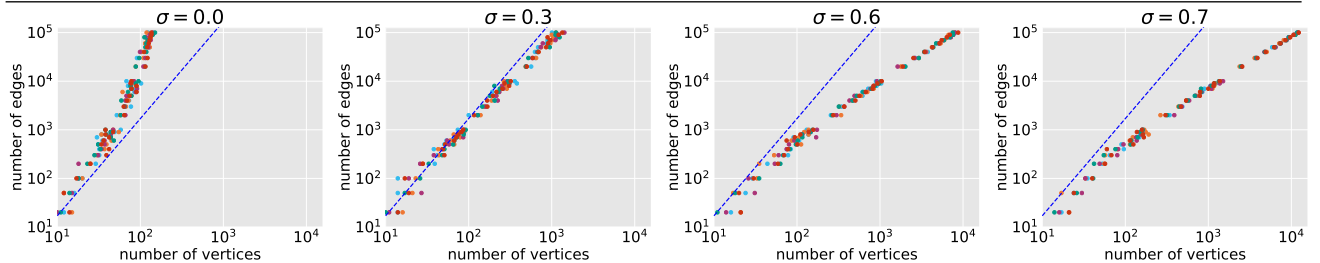


Figure (1): Relationship between the number of edges and the number of vertices in DYNPAND multigraphs generated according to Equation (4), for various values of σ . Plots are shown on a log-log scale. Different colors correspond to different random seeds. The blue dashed line has a slope of 2, indicating a quadratic relationship. We see the multigraphs become increasingly sparse as σ increases.

Assumption 1. The decay function f_2 in Equation 4 satisfies $\sum_{i=1}^j f_2(d_{i,j}) \leq D$ for some $D < \infty$ and all j .

Remark. The condition $\sum_{i=1}^j f_2(d_{i,j}) \leq D$ is easily satisfied provided the rate of arrival of edges is bounded. For example, if f_2 is a window function of size w , then D is the maximum number of edges arriving in a period of length w . If f_2 is an exponential function, $f_2(d) = e^{-d/\lambda}$, and m is the maximum number of edges arriving per unit time, then

$$\sum_{i < j} f_2(d_{i,j}) \leq \sum_{i < j} e^{-\lfloor d_{i,j} \rfloor / \lambda} \leq \sum_{\ell=0}^{\infty} m e^{-\ell/\lambda} = \frac{m e^{-\lambda}}{e^{-\lambda} - 1}$$

where the final inequality is due to the fact that there are at most m observations with $\lfloor d_{i,j} \rfloor = \ell$ for $\ell = 1, \dots, \infty$. If f is a logistic function, $f(d) = e^{-d+\lambda} / (1 + e^{-d+\lambda})$, then $\sum_{i < j} f(d_{i,j})$ is bounded above by $\sum_{\ell=0}^{\infty} e^{\lambda} e^{-\ell} = e^{\lambda+1} / (e - 1)$.

Theorem 1. If f_2 satisfies Assumption 1, and if $\sigma > 0.5$, the model described by Equation (4) is sparse.

Before proving Theorem 1, we introduce some lemmas that are required for our main result.

Lemma 2. If the decay function of a ddCRP satisfies Assumption 1, the number of clusters grows linearly in the number of observations, n .

Proof. The probability of the i -th observation starting a new cluster is $\frac{\tau}{\tau + \sum_{j < i} f(d_{i,j})}$, therefore the expected number of clusters in n observations is

$$\mathbb{E}[K_n] = \sum_{i=1}^n \frac{\tau}{\tau + \sum_{j < i} f(d_{i,j})} \geq \frac{n\tau}{\tau + b}$$

□

Next, define a hierarchical Pitman-Yor ddCRP as a time-dependent clustering model for grouped data. Let x^1, \dots, x^K represent K data groups, where $x^k = (x_1^k, \dots, x_{n_k}^k)$ contains n_k observations. Associate with

each observation x_i^k a table indicator b_i^k , and associate with the c -th table in group k a dish $\phi_{k,c}$, according to

$$\begin{aligned} H &\sim \text{PY}(\gamma, \sigma, \Theta) \\ P(b_i^k = c | z_{<i}^k, \tau) &\propto \begin{cases} \sum_{j: b_j^k = c} f_2(d_{i,j}) & c \leq C_+^k \\ \tau & c = C_+^k + 1 \end{cases} \\ \phi_{k,c} &\sim H, \quad \theta_i^k = \phi_{k, b_i^k}. \end{aligned} \quad (6)$$

observations with the same value of θ_i^k belong to the same cluster. This formulation is a slight variation on the spatial ddCRP of Ghosh et al. (2011), with a Pitman-Yor process replacing of the top-level DP.

Lemma 3. If the decay function satisfies the condition in Lemma 2, then the number of clusters in the hierarchical Pitman-Yor ddCRP grows as $O(n^\sigma)$.

Proof. Following Lemma 2, the number of tables associated with each group x^k grows linearly in the number n_k of observations in the group, so the total number of tables across all groups grows linearly in the total number $n = \sum_k n_k$ of observations. Tables are then assigned dishes according to a Pitman-Yor CRP (Equation (3)). Under this distribution, the expected number of dishes in k is (Pitman et al., 2002),

$$\frac{\Gamma(\gamma + k + \sigma)\Gamma(\gamma + 1)}{\sigma\Gamma(\gamma + k)\Gamma(\gamma + \sigma)} - \frac{\gamma}{\sigma} \simeq \frac{\Gamma(\gamma + 1)}{\sigma\Gamma(\gamma + \sigma)} k^\sigma.$$

By the law of iterated expectations, the expected number of dishes sampled by n customers grows as $O(n^\sigma)$ for $\sigma > 0$. □

Note that the above proof does not depend on how observations are assigned to groups, and therefore the lemma holds if the groups are assigned via a ddCRP (or other clustering mechanism).

Proof of Theorem 1. Following from Lemma 3, the expected number of distinct vertices grows as $O(n^\sigma)$, where n is the number of edges. The resulting random multigraph is therefore sparse provided $\sigma > 0.5$. □

3.1.1 Empirical evaluation of sparsity

In Figure (1), we empirically investigate the effect of σ on the sparsity of multigraphs generated according to Equation (4). Recall that a model is considered sparse if the number of edges grows subquadratically with the number of vertices. Figure (1) plots the number of edges and number of vertices (on a log-log scale) for multigraphs with $\alpha = 1$, $\gamma = 1$, $\tau = 0.2$, and various values of σ . Each dot represents a single sampled multigraph, and the blue dashed line has slope 2—providing the boundary between sparse and dense graphs. We see that, for $\sigma > 0.5$, the number of edges grows subquadratically with the number of vertices, as expected according to Theorem 1. As we decrease σ , the graphs become denser. With $\sigma = 0.3$, the number of edges is approximately quadratic in the number of vertices. With $\sigma = 0$, corresponding to a DP-distributed base measure, the number of edges is superquadratic in the number of vertices.

3.2 Discussion of modeling choices

A number of dynamic extensions to the Dirichlet process have been proposed, that could be used to introduce temporal dependency into the MDND. We choose the ddCRP for three reasons. First, it allows us to guarantee sparsity, as described in Section 3.1. Second, it captures behavior that we are likely to see in a dynamic network context: recent communications are likely to be more influential than more distant communications. Finally, its construction easily lends itself to an easy-to-implement sampler, as described in Section 4; by contrast, many other dependent Dirichlet processes have much more complicated inference algorithms, which would limit scalability.

A known limitation of the ddCRP is that it assumes that all data has been observed up to the current time point; the distribution is not invariant to adding edges at previously observed time points. This is not a concern in our setting, since we are typically able to observe past instances of the full graph, and are interested in predicting future edges.

We note that the hierarchical structure over the cluster-specific distributions is similar to the spatial ddCRP proposed by Ghosh et al. (2011), where a collection of ddCRPs are coupled using a shared Dirichlet process. We choose to use a Pitman-Yor process in place of the Dirichlet process to ensure sparsity. Alternative heavy-tailed nonparametric distributions such as the normalized generalized gamma process could be used in place of the Pitman-Yor process; we chose the Pitman-Yor process for ease of inference.

Algorithm 1 Dynamic Nonparametric Network Distribution Inference

Input: Sequence $E = (e_1, e_2, \dots)$, $\alpha_0, \gamma_0, \tau_0, \sigma_0$

- 1: Compute distances $\{d_{i,j}\}$ ▷ Equation (5)
- 2: **for** epoch= 1, 2, ..., max_epoch **do**
- 3: **for** $i = 1, \dots, n$ **do**
- 4: Sample $z_i | z_{<i}, s_i, r_i \dots$ ▷ Equation (7)
- 5: Sample $b_i^s | s_i, z_i, \dots$ ▷ Equation (9)
- 6: Sample $b_i^r | r_i, z_i, \dots$ ▷ Equation (9)
- 7: **end for**
- 8: Sample $\alpha, \gamma, \tau, \sigma$ via random walk Metropolis Hastings
- 9: **end for**

4 Inference

Conditioned on the hyperparameters, we can directly generate samples from the posterior by sequentially sampling cluster assignments. Let b_i^s and b_i^r be the table assignments of the i -th sender and recipient, respectively. As we proceed, let K_+ indicate the total number of clusters seen so far; V_+ be the total number of vertices seen so far; and ρ_v be the total number of tables so far associated with vertex v . We can sample the i -th cluster assignment, given the previous assignments, as

$$P(z_i = k | s_i, r_i) \propto P(s_i | z_i = k) P(r_i | z_i = k) P(z_i = k | z_{<i}) \quad (7)$$

where

$$P(s_i = v | z_i = k) = \begin{cases} \frac{\sum_{j:j<i, z_j=k, s_j=v} g(d_{i,j})}{\tau + \sum_{j:j<i, z_j=k} g(d_{i,j})} \\ + \frac{\tau}{\tau + \sum_{j:j<i, z_j=k} g(d_{i,j})} \frac{\rho_v - \sigma}{\sum_v \rho_v + \gamma} & v \leq V_+ \\ \frac{\tau}{\tau + \sum_{j:j<i, z_j=k} g(d_{i,j})} \frac{\gamma + V\sigma}{\sum_v \rho_v + \gamma} & v = V_+ + 1 \end{cases}$$

$$P(z_i = k | z_{<i}) \propto \begin{cases} \sum_{j:j_j=k} f_1(d_{i,j}) & k \leq K_+ \\ \alpha & k = K_+ + 1 \end{cases} \quad (8)$$

and $P(r_i = v | z_i = k)$ is defined analogously to $P(s_i = v | z_i = k)$. Conditioned on the cluster assignment, we sample a table b_i^s for the sender as

$$P(b_i^s = c | s_i, z_i) \propto \begin{cases} \sum_{\substack{j:z_j=z_i, \\ s_j=s_i, b_j^s=c}} f_2(d_{i,j}) & \text{existing table} \\ \frac{\rho_{s_i} - \sigma}{\sum_v \rho_v + \gamma} & \text{new table} \end{cases} \quad (9)$$

Once we have sampled the complete set of assignments, we can sample the hyperparameters using Metropolis Hastings steps (see Blei & Frazier (2011) for details on evaluating the likelihood for the ddCRP). We alternate between these two steps until convergence. The procedure is summarized in Algorithm 1.

Table (1): Predictive log likelihood of held-out edges on four real-world datasets (mean \pm standard deviation over time slots).

Method	MDND (CRP)	DyNPAND-WINDOW	DyNPAND-LOGISTIC	DyNPAND-EXPONENTIAL
CollegeMsg	-1084.37 \pm 18.73	-716.80 \pm 9.72	-665.45\pm10.78	-686.21 \pm 11.04
Email-Eu	-25364.11 \pm 355.17	-15151.65 \pm 206.36	-14672.37 \pm 279.81	-14289.64\pm223.70
SocialEv	-872.73 \pm 53.41	-577.06\pm42.54	-595.81 \pm 41.64	-586.57 \pm 41.97
DBLP	-906.00 \pm 37.27	-559.83 \pm 23.35	-565.58 \pm 23.46	-558.53\pm23.21

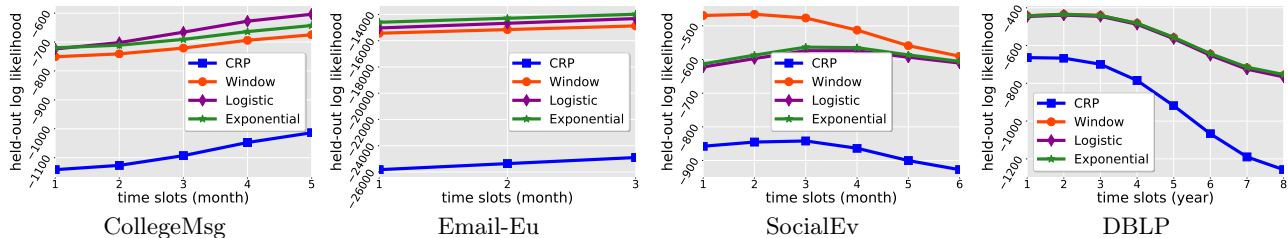


Figure (2): Predictive log likelihood vs. time slots. Each evaluation is the average value over 20 samples.

5 Experiments

In this section, we address the following questions: (1) How well does DyNPAND capture the underlying multi-graph behavior to predict unseen held-out edges? and (2) How accurate is DyNPAND in terms of forecasting future interactions, compared to state-of-the-art dynamic interaction graph models?

Datasets. We evaluated our model on four real-world temporal multigraphs:

- *CollegeMsg network*² (Panzarasa et al., 2009) records private messages in an online social multigraph at the University of California, Irvine, with 1,899 vertices and 20,296 interactions over 193 days. The average monthly sparsity is 0.013.
- *Email-Eu-core temporal network*³ (Paranjape et al., 2017) consists of all incoming and outgoing emails in a large European research institution. 986 individuals exchange 332,334 separate e-mails over 803 days. We considered a subset of the first 3 months, with 49,282 edges and 702 vertices, with an average monthly sparsity of 0.028.
- *Social Evolution network (SocialEv)*⁴ (Madan et al., 2011) tracks the everyday life of 70 students within a dormitory, based on mobile phone data. We consider Bluetooth connections, calls and SMSs as interactions, yielding a multigraph high clustering coefficient and about 1M events over six months. We sampled a subset of edges, which resulted in 6,140 edges and 323 vertices, with average monthly sparsity of 0.414.

²<http://snap.stanford.edu/data/CollegeMsg.html>

³<http://snap.stanford.edu/data/email-Eu-core-temporal.html>

⁴<http://realitycommons.media.mit.edu/socialrevolution.html>

- *DBLP* (Asur et al., 2009) contains coauthorship information for more than 800,000 computer science publications among 958 authors over ten years (1997-2006). We consider the 324 most connected authors, yielding a multigraph with 11,154 edges and average annual sparsity of 0.022.

Experimental setting. For DyNPAND, we considered three decay functions: (1) WINDOW decay: $f(d) = 1[d < \lambda]$ only considers dependency with edges that are distant at most λ from the current edge, (2) EXPONENTIAL decay: $f(d) = e^{-d/\lambda}$ decays exponentially with time, and (3) LOGISTIC decay: $f(d) = \frac{e^{-d+\lambda}}{1+e^{-d+\lambda}}$ is a smooth version of the window decay. We used the same decay function for f_1 and f_2 . We explored several values for λ and found that $\lambda = 5$ for window decay and $\lambda = 1.5$ for other decays work well on all datasets. We ran all algorithms for 100 iterations for each dataset. We used Gamma(5,1) priors for α , β , and τ , and a Beta(1,1) prior for σ .

Baselines. For the held-out edge prediction task, we compared against the (stationary) MDND, described in Section 2.1.1. We implemented MDND using the inference algorithm in Section 4, with $\sigma = 0$ and $d_{i,j} = 1$ for all $i \geq j$; we found that this algorithm gave comparable results to the implementation of Williamson (2016). For the graph forecasting task, we also compared against three recent Bayesian dynamic network models, introduced in Section 2.2: the dynamic relational gamma process model (DRGPM, Yang & Koepl, 2018a), the dynamic Poisson gamma model (DPGM, Yang & Koepl, 2018b), and the dynamic gamma process Poisson factorization (DGPPF, Acharya et al., 2015). These models are not applicable to the held-out edge prediction task, since they assume all vertices are observed. However, they can be used to predict the

Table (2): MAP@k for the future interaction prediction task (mean value over time slots).

MAP@k	DYNPAND			MDND			DRGPM			DPGM			DGPPF		
	@10	@50	@100	@10	@50	@100	@10	@50	@100	@10	@50	@100	@10	@50	@100
COLLEGE MSG	0.466	0.504	0.516	0.267	0.295	0.321	0.118	0.091	0.085	0.037	0.071	0.067	0.052	0.085	0.065
EMAIL-EU	0.390	0.452	0.585	0.238	0.227	0.351	0.330	0.464	0.494	0.308	0.451	0.490	0.199	0.380	0.451
SOCIALEV	0.586	0.515	0.423	0.179	0.162	0.253	0.001	0.008	0.009	0.033	0.011	0.024	0.008	0.014	0.021
DBLP	0.493	0.496	0.492	0.205	0.118	0.241	0.388	0.459	0.451	0.451	0.516	0.498	0.374	0.485	0.476

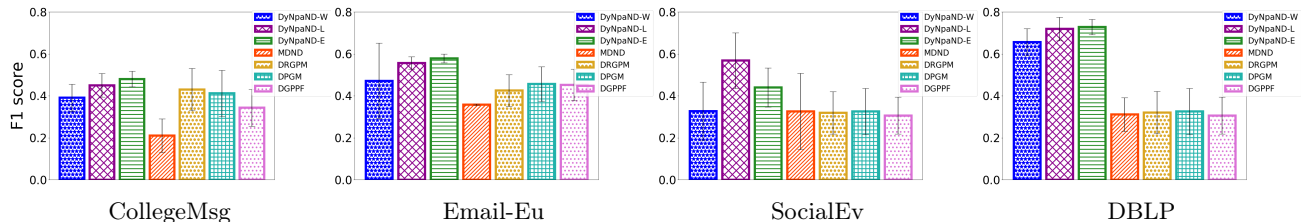


Figure (3): F1 score for future interaction prediction. Decay functions for DYNPAND are WINDOW (W), EXPONENTIAL (E), and LOGISTIC (L) (averaged over time slots).

entire graph at the next time slot over seen vertices. We modify this distribution to be appropriate to our forecasting task by predicting the n_T edges with the highest probability at time slot T .

5.1 Prediction of held-out edges

A common method to evaluate a Bayesian model is to infer a distribution over parameters given an incomplete training set, and look at the probability of the unseen held-out set given that distribution. The higher the likelihood of the held-out set values, the better the model performance.

To evaluate DYNPAND on this task, we split each data set into time slots (one month for CollegeMsg, Email-Eu-core, and SocialEv; one year for DBLP), and train on 85% of interactions in each time slot. We estimate the log predictive likelihood of the remaining interactions using a “Left-to-Right” evaluation algorithm (Wallach et al., 2009).

Table (1) shows the predictive log likelihood computed by DYNPAND using three different decays (*i.e.* WINDOW, EXPONENTIAL and LOGISTIC) in comparison with the CRP decay function used in Williamson (2016) on four real multigraphs. We see that in each case, all three dynamic DYNPAND multigraphs outperform the stationary MDND. In Figure (2), we illustrate the predictive log likelihood per time slot. Again, we see that DYNPAND outperforms the stationary MDND model across all time slots. This demonstrates that considering important properties observed in real-world data (*i.e.* time dependency and sparsity) results in a better log likelihood.

5.2 Forecasting future interactions

Held-out set log likelihood is useful for evaluating whether the model is a good fit for data. However, in practical applications we often want to make concrete predictions of future interactions. Given all interactions up to time slot $T - 1$, we want to predict the edges arriving at time slot T . We assume that we know the number of edges, n_T , and wish to predict their location. For performance comparison, we look at the F1 score and MAP@k. F1 score is $2 \times (\text{precision} \times \text{recall}) / (\text{precision} + \text{recall})$. Precision is the fraction of edges in the predicted graph present in the true graph, and recall is the fraction of edges of the true graph present in the predicted graph. MAP@k is the classical mean average precision measure. We calculated values based on 10 posterior samples.

Table (2) shows the MAP@k for DYNPAND and the four comparison methods. For space reasons, the numbers reported for DYNPAND represent the best result of the three decay functions; more complete tables are included in Appendix A. Figure (3) summarizes the corresponding F1 scores.

The results show that DYNPAND performs comparably or better on both metrics across all datasets. We hypothesize that this is due to several reasons. First, DYNPAND is explicitly designed in terms of a predictive distribution over edges, making it well-suited to predicting future edges. Second, DYNPAND is able to increase the number of vertices over time, and is likely better able to capture natural multigraph growth. Conversely, the other methods assume the number of vertices is fixed—and explicitly incorporate the absence of edges at earlier time points into the likelihood. Third, unlike the other methods, DYNPAND allows us

to capture sparsity; if the multigraph is sparse, then this should lead to a more accurate model.

6 Discussion

We have presented a new distribution for temporally varying, structured multigraphs, that allows us to represent both sparse and dense networks. Since our model explicitly describes a sequence of edges, it is well-suited to predict future edges. As we saw in Section 5, these properties translate into impressive predictive performance compared with state-of-the-art Bayesian models.

In this paper, we incorporate dynamics using a ddCRP model, which encourages edges to belong to clusters that have been recently active. An interesting avenue for future research would be to explore alternative forms of dependency, and incorporate mechanisms that can capture link reciprocity (Blundell et al., 2012).

References

- Acharya, A., Ghosh, J., & Zhou, M. 2015, arXiv preprint arXiv:1512.08996
- Airoldi, E. M., Blei, D. M., Fienberg, S. E., & Xing, E. P. 2008, *Journal of machine learning research*, 9, 1981
- Aldous, D. J. 1981, *Journal of Multivariate Analysis*, 11, 581
- Asur, S., Parthasarathy, S., & Ucar, D. 2009, *ACM Transactions on Knowledge Discovery from Data (TKDD)*, 3, 16
- Blei, D. M. & Frazier, P. I. 2011, *Journal of Machine Learning Research*, 12, 2461
- Blundell, C., Beck, J., & Heller, K. A. 2012, in *Advances in Neural Information Processing Systems*, 2600–2608
- Cai, D., Campbell, T., & Broderick, T. 2016, in *Advances in Neural Information Processing Systems*, 4249–4257
- Caron, F. & Fox, E. B. 2017, *Journal of the Royal Statistical Society: Series B (Statistical Methodology)*, 79, 1295
- Crane, H. & Dempsey, W. 2018, *Journal of the American Statistical Association*, 113, 1311
- Dunlavy, D. M., Kolda, T. G., & Acar, E. 2011, *ACM Transactions on Knowledge Discovery from Data (TKDD)*, 5, 10
- Durante, D. & Dunson, D. B. 2014, *Biometrika*, 101, 883
- Foulds, J., DuBois, C., Asuncion, A., Butts, C., & Smyth, P. 2011, in *Proceedings of the Fourteenth International Conference on Artificial Intelligence and Statistics*, 287–295
- Fu, W., Song, L., & Xing, E. P. 2009, in *Proceedings of the 26th annual international conference on machine learning*, 329–336
- Ghalebi, E., Mirzasoleiman, B., Grosu, R., & Leskovec, J. 2018, in *Advances in Neural Information Processing Systems*, 9862–9872
- Ghosh, S., Ungureanu, A. B., Sudderth, E. B., & Blei, D. M. 2011, in *Advances in Neural Information Processing Systems*, 1476–1484
- Gopalan, P., Hofman, J. M., & Blei, D. M. 2015, in *UAI*, 326–335
- Guo, F., Hanneke, S., Fu, W., & Xing, E. P. 2007, in *Proceedings of the 24th international conference on Machine learning*, ACM, 321–328
- Heaukulani, C. & Ghahramani, Z. 2013, in *International Conference on Machine Learning*, 275–283
- Ho, Q., Song, L., & Xing, E. 2011, in *Proceedings of the Fourteenth International Conference on Artificial Intelligence and Statistics*, 342–350
- Hoover, D. 1979, Preprint. Institute for Advanced Study, Princeton.
- Karrer, B. & Newman, M. 2011, *Physical Review E*, 83, 016107
- Kemp, C., Tenenbaum, J., Griffiths, T., Yamada, T., & Ueda, N. 2006, in *National Conference on Artificial Intelligence (AAAI)*, 381–388
- Kim, M. & Leskovec, J. 2013, in *Advances in neural information processing systems*, 1385–1393
- Lee, J., James, L. F., Choi, S., & Caron, F. 2018, arXiv preprint arXiv:1810.01778
- Lin, D., Grimson, E., & Fisher, J. W. 2010, in *Advances in neural information processing systems*, 1396–1404
- MacEachern, S. N. 2000, Unpublished manuscript, Department of Statistics, The Ohio State University, 1
- Madan, A., Cebrian, M., Moturu, S., Farrahi, K., et al. 2011, *IEEE Pervasive Computing*, 11, 36
- Miller, K., Jordan, M. I., & Griffiths, T. L. 2009, in *Advances in neural information processing systems*, 1276–1284
- Ng, Y. C. & Silva, R. 2017, arXiv:1710.04008
- Orbanz, P. & Roy, D. M. 2014, *IEEE Transactions on Pattern Analysis and Machine Intelligence*, 37, 437
- Palla, K., Caron, F., & Teh, Y. W. 2016, arXiv preprint arXiv:1607.01624
- Panzarasa, P., Opsahl, T., & Carley, K. M. 2009, *Journal of the American Society for Information Science and Technology*, 60, 911

- Paranjape, A., Benson, A. R., & Leskovec, J. 2017, in Proceedings of the Tenth ACM International Conference on Web Search and Data Mining, ACM, 601–610
- Pitman, J., Yor, M., et al. 1997, The Annals of Probability, 25, 855
- Pitman, J. et al. 2002, Combinatorial stochastic processes, Tech. rep., Technical Report 621, Dept. Statistics, UC Berkeley, 2002. Lecture notes for . . .
- Ren, L., Dunson, D. B., & Carin, L. 2008, in Proceedings of the 25th International Conference on Machine Learning, ICML '08, New York, NY, USA, 824–831
- Snijders, T. & Nowicki, T. 1997, Journal of Classification, 14, 75
- Wallach, H. M., Murray, I., Salakhutdinov, R., & Mimno, D. 2009, in Proceedings of the 26th Annual International Conference on Machine Learning, 1105–1112
- Williamson, S. A. 2016, The Journal of Machine Learning Research, 17, 7102
- Xing, E. P., Fu, W., Song, L., et al. 2010, The Annals of Applied Statistics, 4, 535
- Xu, K. 2015, in International Conference on Artificial Intelligence and Statistics, 1079–1087
- Xu, K. S. & Hero, A. O. 2014, IEEE Journal of Selected Topics in Signal Processing, 8, 552
- Yang, S. & Koepl, H. 2018a, in International Conference on Machine Learning, 5547–5556
- Yang, S. & Koepl, H. 2018b, in Thirty-Second AAAI Conference on Artificial Intelligence
- Zhou, M. 2015, in Artificial Intelligence and Statistics, 1135–1143
- Zhou, M. & Carin, L. 2013, IEEE Transactions on Pattern Analysis and Machine Intelligence, 37, 307

Supplementary material

A Additional experimental results

Tables (3), (4) and (5) expand Table (2) to include standard deviation across 10 repeats. Table (6) shows results for each of the three decay functions.

Table (3): MAP@10

Method	DyNpAND	MDND	DRGPM	DPGM	DGPPF
COLLEGE _{MSG}	0.466±0.030	0.267±0.132	0.118±0.105	0.037±0.007	0.052±0.016
EMAIL-EU	0.390±0.052	0.238±0.101	0.330±0.124	0.308±0.110	0.199±0.099
SOCIAL _{EV}	0.586±0.338	0.179±0.104	0.001±0.000	0.033±0.008	0.008±0.003
DBLP	0.493±0.274	0.205±0.039	0.388±0.263	0.451±0.228	0.374±0.204

Table (4): MAP@50

Method	DyNpAND	MDND	DRGPM	DPGM	DGPPF
COLLEGE _{MSG}	0.504±0.033	0.295±0.118	0.091±0.060	0.071±0.064	0.085±0.070
EMAIL-EU	0.452±0.012	0.227±0.097	0.464±0.112	0.451±0.091	0.380±0.087
SOCIAL _{EV}	0.515±0.232	0.162±0.239	0.008±0.003	0.011±0.009	0.014±0.006
DBLP	0.496±0.143	0.118±0.019	0.459±0.254	0.516±0.229	0.485±0.197

Table (5): MAP@100

Method	DyNpAND	MDND	DRGPM	DPGM	DGPPF
COLLEGE _{MSG}	0.516±0.026	0.321±0.065	0.085±0.052	0.067±0.061	0.069±0.065
EMAIL-EU	0.585±0.036	0.318±0.125	0.494±0.117	0.490±0.104	0.451±0.091
SOCIAL _{EV}	0.423±0.151	0.253±0.169	0.009±0.004	0.024±0.010	0.021±0.006
DBLP	0.492±0.111	0.241±0.012	0.451±0.234	0.498±0.208	0.476±0.181

Table (6): Map@k of three decay functions

MAP@k	DyNpAND-WINDOW			DyNpAND-LOGISTIC			DyNpAND-EXPONENTIAL		
	@10	@50	@100	@10	@50	@100	@10	@50	@100
COLLEGE _{MSG}	0.47±0.03	0.50±0.03	0.52±0.03	0.46±0.15	0.50±0.09	0.51±0.14	0.46±0.11	0.48±0.11	0.49±0.15
EMAIL-EU	0.25±0.04	0.39±0.01	0.46±0.09	0.33±0.08	0.43±0.04	0.50±0.10	0.39±0.05	0.45±0.01	0.50±0.04
SOCIAL _{EV}	0.34±0.16	0.32±0.02	0.28±0.03	0.50±0.36	0.51±0.30	0.49±0.27	0.59±0.34	0.51±0.23	0.42±0.15
DBLP	0.39±0.11	0.42±0.07	0.45±0.05	0.46±0.14	0.40±0.07	0.49±0.05	0.49±0.27	0.50±0.14	0.49±0.11

B Notation

In Table 7, we summarize the notation used in the main paper.

Table (7): Table of notation used in the paper

s_i, r_i	sender and receiver of edge i
z_i	cluster of edge i
α	concentration parameter of DP/ddCRP over clusters
γ	concentration parameter of global DP/PYP
τ	concentration parameter of cluster-specific DP/ddCRP
σ	discount parameter of global DP/PYP
A_k	DP over senders (outgoing vertices) of cluster k
B_k	DP over recipients (ingoing vertices) of cluster z
$d_{i,j}$	distance i th and j th edges
$f_1(\cdot)$	decay function associated with ddCRP over clusters
$f_2(\cdot)$	decay function associated with cluster-specific ddCRPs
K_+	total number of observed clusters
V_+	total number of observed vertices
ρ_v	number of tables associated with vertex v
b_i^s (b_i^r)	table associated with i th sender (recipient)